A model study of the circulation in the Pearl River Estuary (PRE) and its adjacent coastal waters: 2. Sensitivity experiments

L. A. Wong,[1] J. C. Chen,[1] H. Xue,[2] L. X. Dong,[3] W. B. Guan,[1] and J. L. Su[3]

Received 22 April 2002; revised 19 January 2003; accepted 26 February 2003; published 23 May 2003.

[1] The Princeton Ocean Model is used to study the circulation in the Pear River Estuary (PRE) and the adjacent coastal waters in the winter and summer seasons. *Wong et al.* [2003] compares the simulation results with the in situ measurements collected during the Pearl River Estuary Pollution Project (PREPP). In this paper, sensitivity experiments are carried out to examine the plume and the associated frontal dynamics in response to seasonal discharges and monsoon winds. During the winter, convergence between the seaward spreading plume water and the saline coastal water sets up a salinity front that aligns from the northeast to the southwest inside the PRE. During the summer the plume water fills the PRE at the surface and spreads eastward in the coastal waters in response to the prevailing southwesterly monsoon. The overall alignment of the plume is from the northwest to the southeast. The subsurface front is similar to that in the winter and summer except that the summer front is closer to the mouth and the winter front closer to the head of the estuary. Inside the PRE, bottom flows are always toward the head of the estuary, attributed to the density gradient associated with the plume front. In contrast, bottom flows in the shelf change from offshore in winter to onshore in summer, reflecting respectively the wintertime downwelling and summertime upwelling. Wind also plays an essential role in controlling the plume at the surface. An easterly wind drives the plume westward regardless winter or summer. The eastward spreading of the plume during the summer can be attributed to the southerly component of the wind. On the other hand, the surface area of the plume is positively proportional to the amount of discharge. *INDEX TERMS:* 4532 Oceanography: Physical: General circulation; 4255 Oceanography: General: Numerical modeling; 4235 Oceanography: General: Estuarine processes; *KEYWORDS:* estuary, coastal circulation, front, observation, modeling

Citation: Wong, L. A., J. C. Chen, H. Xue, L. X. Dong, W. B. Guan, and J. L. Su, A model study of the circulation in the Pearl River Estuary (PRE) and its adjacent coastal waters: 2. Sensitivity experiments, *J. Geophys. Res.*, *108*(C5), 3157, doi:10.1029/2002JC001452, 2003.

1. Introduction

[2] The circulation is a fundamental factor that controls a significant amount of the variability of water quality and suspended sediment transport in the estuaries. The circulation in the Pearl River Estuary (PRE) is very complex owing to its complicated topography and multiple forcing factors such as river outflows, tides, monsoons, and coastal currents. The circulation patterns are largely distinct between the summer and the winter because of the seasonal river discharge and seasonal climate. There have been a few numerical investigations on the circulations in the PRE and its adjacent coastal waters. They are, however, limited to mostly tidal currents in the estuary [e.g., *Ye et al.*, 1986; *Ye and Preiffer*, 1990; *Huang et al.*, 1992; *Wang et al.*, 1992; *Hu*, 1995], which is obviously insufficient for understanding the hydrodynamic characteristics and their variations in the PRE.

[3] *Wong et al.* [2003] used a 3D estuarine and coastal ocean model to simulate the circulation in the PRE and its adjacent coastal waters. The model results were verified using the observations from the Pearl River Estuary Pollution Project (PREPP) field surveys in July 1999 and January 2000. In summary, the Pearl River outflow forms a plume and an associated frontal zone in the study area. In the winter, this frontal zone is inside the estuary from the surface to the bottom. In the summer, however, the subsurface front remains inside of the PRE, while the surface front moves out of the estuary because of the excessive freshwater discharge and the southwesterly wind. The vertical distribution of the halocline along the main axis of the estuary indicates a two–layer gravitational circulation associated with the plume frontal zone with the seaward surface flows and the up-the-estuary flows at depth.

[1]Center for Coastal and Atmospheric Research, Hong Kong University of Science and Technology, Kowloon, Hong Kong.
[2]School of Marine Sciences, University of Maine, Orono, Maine, USA.
[3]Marine Modeling Laboratory, Second Institute of Oceanography, State Oceanic Administration, Hangzhou, China.

0148-0227/03/2002JC001452$09.00

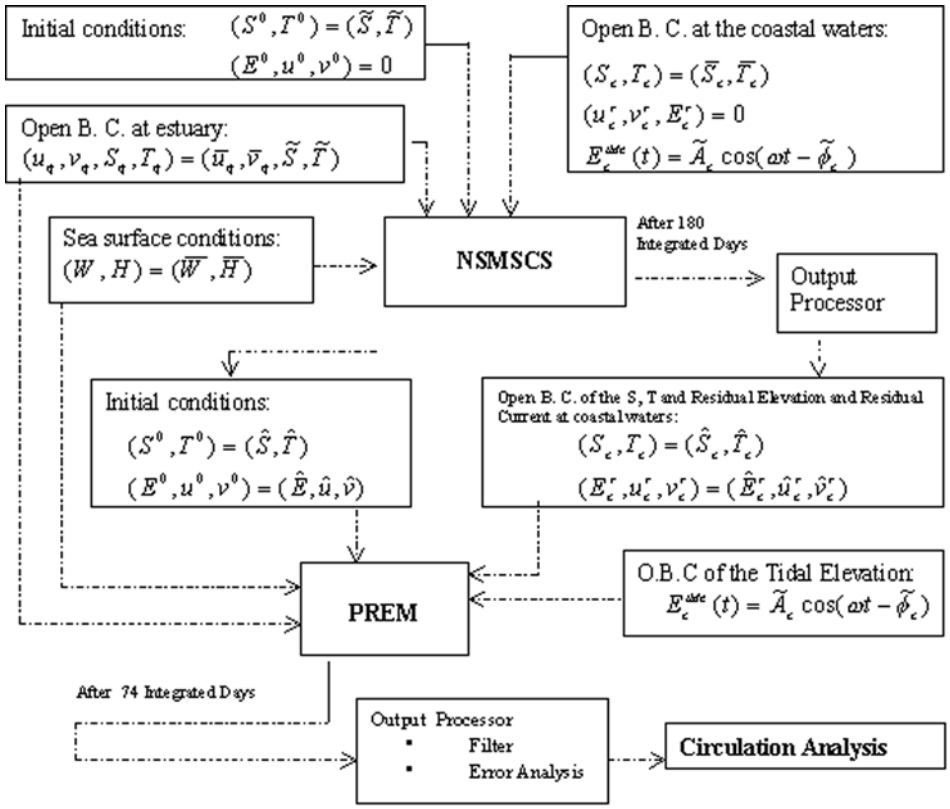

Figure 1. The flowchart of the nested system.

[4] Furthermore, both the observations and the modeled results show that the PRE is a stratified estuary. In particular, the stratification is intensified during the summer, and it can extend into the coastal waters outside of the estuary because of the larger river discharge and the southwesterly monsoon wind. Although the tidal amplitude is small in the PRE, the tidal mixing plays a very significant role in affecting the salinity distribution, especially during the spring tide in the winter. In winter, stratification is relatively strong during the neap tide when the surface-to-bottom salinity difference varies from 10 ppt to 15 ppt over the course of a tidal cycle. However, during the spring tide the stratification that occurred during the neap tide is eroded and the salinity difference from the surface to the bottom is less than 2 ppt over a tidal cycle. In this study, we will focus on examining numerically the patterns, variations and dominant factors of the seasonal general circulation of the PRE and its coastal waters on the basis of the hydrodynamic model discussed by *Wong et al.* [2003].

2. Experiment Design

[5] The Pearl River Estuary Model (PREM) is nested in the larger-scale North Shelf Model of the South China Sea (NSMSCS). Figure 1 shows the flowchart of the nested system, in which the over caps "-","∼", and "^" denote the climatological monthly average, the estimated value based on historical observations, and the output from the NSMSCS, respectively. The subscripts "q" and "c" represent the open boundary at the head of the river and in the coastal waters; the superscripts "0" and "r" represent the initial value and the residual after filtering the tide. There are errors in the NSMSCS, especially near its open boundaries, because of the use of climatological and estimated values. The nested PREM is thus placed far away from the boundary region of the NSMSCS in order to reduce the influence from these boundary errors. The NSMSCS can reach an equilibrium after running the model for 160 days, and thus the results after 180 days are used to initialize and to specify the open boundary condition for the PREM.

[6] The steady barotropic and baroclinic processes can be reached in the PREM after 20 and 60 days of simulation, respectively. Results after day 70 from the PREM are thus analyzed. The residual currents are obtained by using a low-pass filter with a smooth operator of $(a_{24}/24)^2(a_{25}/25)$, where 'a' represents the sum, and the subscripts denote the number of the values used in the sum [*Chen*, 1980].

[7] Several sensitivity experiments are carried out for the winter and the summer simulations, and they are summarized in Tables 1 and 2, respectively. The first experiment for the winter (Table 1) is the default case that considers all

Table 1. Summary of the Sensitivity Experiments for the Winter Simulation[a]

Experiment	River Discharge	Pressure Gradient	Tide	Wind	Residual Circulation
1	Y	Y	Y	Y	$\vec{V}_w$
2	Y	N	Y	Y	$\vec{V}_w^{bt}, \vec{V}_w^{bc}$
3	N	N	Y	N	$\vec{V}_w^{t}$

[a]"Y" means that the effect is considered in the model and "N" means that the effect is excluded from the model.

Table 2. Similar to Table 1 But for the Summer Sensitivity Experiments

Experiment	River Discharge	Pressure Gradient	Tide	Wind	Residual Circulation
1	Y	Y	N	N	$\vec{V}_{sp}$
2	Y	N	N	N	$\vec{V}_{sp}^{bt}, \vec{V}_{sp}^{bc}$
3	Y	Y	Y	N	$\vec{V}_{sp} + \vec{V}_{s}^{t}$
4	Y	Y	Y	Y	$\vec{V}_{s}$
5	Y	N	Y	Y	$\vec{V}_{s}^{bt}, \vec{V}_{s}^{bc}$

the forcings including tide, river discharge, wind and heat flux, and the coastal current. The model output is low-pass filtered to obtain the subtidal circulation ($\vec{V}_W$). In the second experiment, the density gradient term is omitted from the momentum equation, though the density field still evolves with time, which can affect the mixing. The output is again low-pass filtered to obtain a tidal residual, designated as the "barotropic" solution ($\vec{V}_w^{bt}$). Note that the "barotropic" solution is, strictly speaking, "zero density gradient" solution (i.e., the portion of the circulation driven by forces other than the density gradient). The difference between the subtidal circulation from the first and the second experiment represents the portion of the circulation driven by the density gradient force, designated as the "baroclinic" solution ($\vec{V}_w^{bc}$). The third experiment is similar to the second experiment except that the wind is turned off. The low-pass filtered solution from this experiment represents the nonlinear tidal effects in the presence of the background stratification.

[8] For the summer (Table 2), the first two experiments focus on the effects of river discharge, in which both the tide and the wind are turned off. The density gradient term is omitted in the second experiment in order to separate the portion of the circulation that is driven by the density gradient associated with the river plume, $\vec{V}_{sp}^{bc}$. Tide is added in the third experiment to show the modification to the subtidal circulation due to nonlinear tidal effects. Wind effects on the spread of the diluted water in the estuary and in the coastal waters are demonstrated in the forth and fifth experiments, in which southwesterly wind of 3.25 m s^{-1} and 5 m s^{-1} is applied at the surface, respectively. In the sixth experiment, the density gradient term is again omitted from the momentum equation to separate the density-driven circulation ($\vec{V}_s^{bc}$) from its other components ($\vec{V}_s^{bt}$).

3. Winter Circulation

3.1. Horizontal Patterns of the Winter Circulation

[9] Figure 2 shows the subtidal winter circulation and the contributions to the winter circulation from the "barotropic" forcing, the density gradient, and the nonlinear tidal residual. The overall surface currents tend to concentrate along the salinity isolines in the axial direction of the estuary and flow toward the sea (Figure 2a). The outflow turns westward after leaving the PRE. The bottom currents inside the PRE, however, flow toward the head of the estuary along the two deep channels (Figure 2b). This implies that a two-layer gravitational circulation exists associated with the river plume. In the coastal waters a westward coastal current is formed along the shoreline because of the Coriolis steering and the northeasterly monsoon. Meanwhile, the downwelling aspect of the coastal circulation is demonstrated.

[10] The area around the Lantau Island is a transition zone between the coastal regime and the estuarine regime. The four groups of islands, namely, the Wanshan, Shanwen, Jiapeng, and Dangan Islands, further complicate the circulation patterns there. However, most of the saline coastal waters enter the PRE at depth mainly through the Lantau and Urmston waterways, while the surface diluted water flows out of the PRE on the western side of the estuary and converges into the westward coastal current. Maximum currents and the maximum horizontal shear occur near the plume frontal zone, and the vertical shear is also stronger in the estuary than in the coastal waters.

[11] In the coastal waters, the "barotropic" circulation (including mostly the tidal residual currents and the wind driven currents) is similar to the overall circulation (Figures 2a, 2b, 2c, and 2d), suggesting that the "barotropic" processes dominate the coastal circulation. However, inside the estuary, the baroclinic component driven by the density gradient dominates the estuarine circulation (Figures 2a, 2b, 2e, and 2f), including both the two-layer gravitational circulation and the strong flow along the front. The nonlinear tidal effect is small during neap tide. However, during the spring tide, the tidal residual current can contribute considerably to the lateral transport along the plume frontal zone (Figure 2g). This means that the tide has two-sided effects: strong tidal mixing reduces the density gradient so that the portion of the current driven by the density gradient decreases during the spring tide (this can be demonstrated by comparing density gradient currents during the spring tide and neap tide). On the other hand, the tidal nonlinearity becomes much stronger near the frontal zone during the spring tide than the neap tide.

3.2. Vertical Features of the Winter Circulation

[12] Figure 3 shows the locations of the cross-section AL and CS in the PRE and coastal waters, and Figure 4 and Figure 5 show the vertical distribution of the winter circulation and its various components corresponding to those shown in Figure 2 along the main axial section AL and the transversal section CS, respectively.

[13] In the estuary, there is a two-layer circulation along the main axis of the estuary with the outgoing surface flow and the intruding bottom flow (Figure 4b). The vertical scale of this circulation is from the surface to the bottom (about 10 m deep), and the horizontal scale is about 70 km from the head of the estuary. However, in the coastal waters, there is a weaker, reversed, two-layer circulation (surface flow is landward and the bottom flow is seaward) (Figure 4b). Its vertical scale is about 30 $\sim$ 50 m. The Lantou channel is the transition zone between the two opposite flowing circulation cells. The former is mainly generated by the density gradient between the plume and the saline coastal water (Figures 4b and 4f) as the barotropic currents in the estuary is downstream (Figure 4d). In contrary, the coastal two-layer circulation can largely be attributed to the temperature gradient between the coastal waters and the shelf waters [see *Wong et al.*, 2003, Figure 11]. Meanwhile, the downwelling driven by the northeasterly monsoon also contributes a small portion to the coastal reversed two-layer circulation in the "barotropic" coastal waters (Figure 4d).

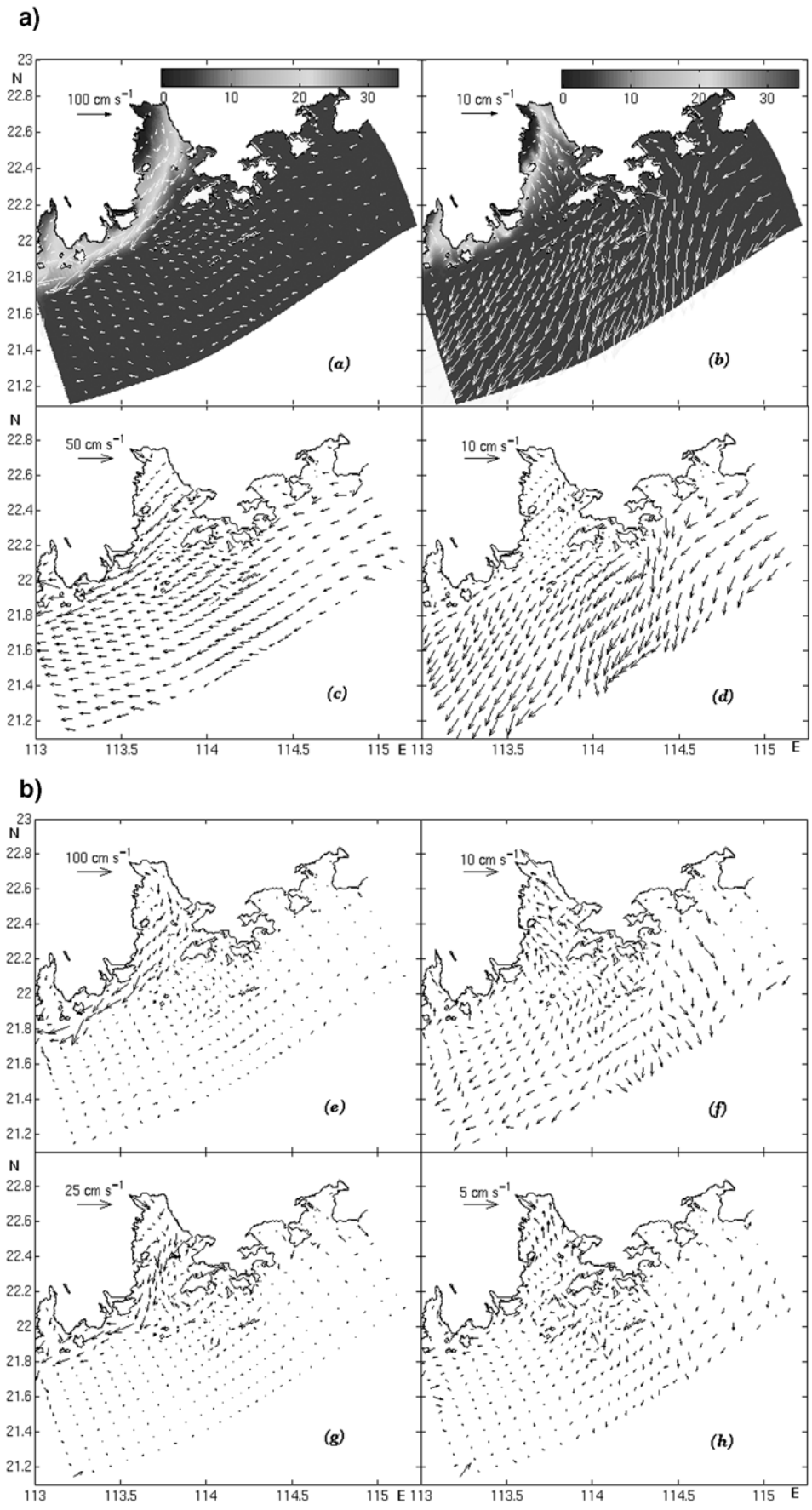
a)
b)
N
E
100 cm s^{-1}
10 cm s^{-1}
50 cm s^{-1}
25 cm s^{-1}
5 cm s^{-1}
0
10
20
30
(a)
(b)
(c)
(d)
(e)
(f)
(g)
(h)
23
22.8
22.6
22.4
22.2
22
21.8
21.6
21.4
21.2
113
113.5
114
114.5
115

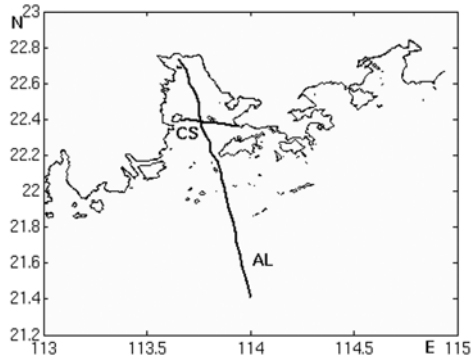

Figure 3. The locations of the cross-section AL and CS in the PRE and coastal waters.

[14] In the estuary, the flow perpendicular to the main axis has the two-layer characteristics as well (surface flow is westward and the bottom flow is eastward) at the head of the estuary (Figures 4a and 4e), but it has a three-layer structure in the area between the Qiao Island and the Neilingding Island (westward at the surface and the bottom, eastward in the mid column). The baroclinic component of the circulation dominates the flow perpendicular to the estuarine axis (Figures 4a and 4e). In the coastal waters, the baroclinic component parallel to the shoreline is weaker than its barotropic counterpart (Figures 4c and 4e), again suggesting that the barotropic process dominates in the coastal waters. The vertical shear of the current is larger in the estuary than in the coastal waters.

[15] The circulation at the transversal section (CS) (Figure 5) shows that: 1) the two-layer gravitational circulation exists primarily in the plume on the western side of the estuary (Figures 5a and 5e) although along this section, the plume occupies almost the entire section except the eastern most 5 km; 2) the two layer circulation is mostly density driven, and the surface seaward current is stronger than the bottom landward current (Figures 5a and 5e); 3) most of the barotropic flow is seaward except the bottom flow in two deep channels (Figure 5c) and similarly, the nonlinear tidal residual is also seaward except in the shallow area between the two channels and in the lower eastern channel (Figure 5g). The transversal baroclinic current has an obvious three-layer structure on the western side of the section (Figures 5b and 5f) with the westward surface and bottom flows and the eastward flow in the mid column, while the transversal barotropic current is mostly westward because of the Coriolis effect. The transversal nonlinear tidal residual, though it is much smaller, is eastward along the section CS. In short, the two-layer gravitational circulation is mostly density driven and it is asymmetric with respect to the main axis of the estuary. Barotropic effects contribute considerably on the eastern side, especially to the transversal flow, because of the Coriolis steering.

4. Summer Circulation

4.1. Horizontal Patterns of the Summer Circulation

[16] The Pearl River discharge reaches its yearly maximum during the summer such that the diluted water almost fills the entire estuary and spreads eastward beyond boundary Hong Kong. Therefore the river discharge plays an exceptionally important role in the summer circulation of the PRE. To illustrate exclusively the density driven current associated with the river plume, the wind and the tide are turned off in the first summer experiment (Figures 6a and 6b), and the ''baroclinic'' contribution driven by the density gradient (Figures 6c and 6d) is separated from the rest of the circulation components (Figures 6e and 6f). Tidal forcing is then added to the summer experiment and Figures 6g and 6h show the modification to the subtidal circulation due to nonlinear tidal effects. Without the wind and the tide (Figures 6a and 6b), it is clear that the surface currents associated with the river plume flow out of the estuary. At the mouth of the PRE, the surface plume is divided into three branches (Figure 6a), among which the westward flowing branch is strongest under the influence of the Coriolis force (Figure 6a). Of the two branches of the surface currents flowing eastward, one passes through the Lantau Channel and continues through the Dangan Channel, and the other through the Urmston Waterway into the Lamma and Tathong Channel. The baroclinic component driven by the density gradient (Figures 6c and 6d) appears to be much larger than its ''barotropic'' counterpart (Figures 6e and 6f) at the surface. Furthermore, the baroclinic process is also responsible for a cyclone eddy near the mouth of the PRE on the western side since it is absent in the barotropic surface circulation shown in Figure 6c. The eddy is a surface feature with a horizontal scale of $\sim$30 km, likely the result from entrainment that occurred near the plume front.

[17] Inside the PRE, the saline coastal waters intrude toward the head of the estuary along the bottom, especially in the two deep channels (Figure 6b). However, the shallow areas are filled with freshwater and the freshwater flows toward the mouth of the estuary. Hence the bottom circulation is more complicated than the surface circulation. The baroclinic component of the bottom circulation is in the same direction (up the estuary) as the total bottom circulation, whereas the barotropic component of the bottom circulation is opposite to that of the total bottom circulation (Figures 6b, 6d, and 6f). The reason is that inside the estuary the density driven circulation dominates. On the other hand, the barotropic component of the bottom circulation dominates in the coastal waters. Although there is no local barotropic forcing in this experiment, the coastal current is

Figure 2. (opposite) The comparison of the winter surface and bottom circulations. (a) The surface general subtidal circulation and the distribution of the surface salinity during the neap tide; (b) the near-bottom (the lowest sigma layer) general subtidal circulation and the distribution of the bottom salinity during the neap tide; (c) and (d) the surface and the bottom ''barotropic'' components of the winter subtidal circulation; (e) and (f) the surface and the bottom circulation driven by density gradient during the neap tide; and (g) and (h) the surface and the bottom subtidal circulation due to nonlinear tidal effects during the spring tide. Plot grid interval: 8 grids $\times$ 8 grids.

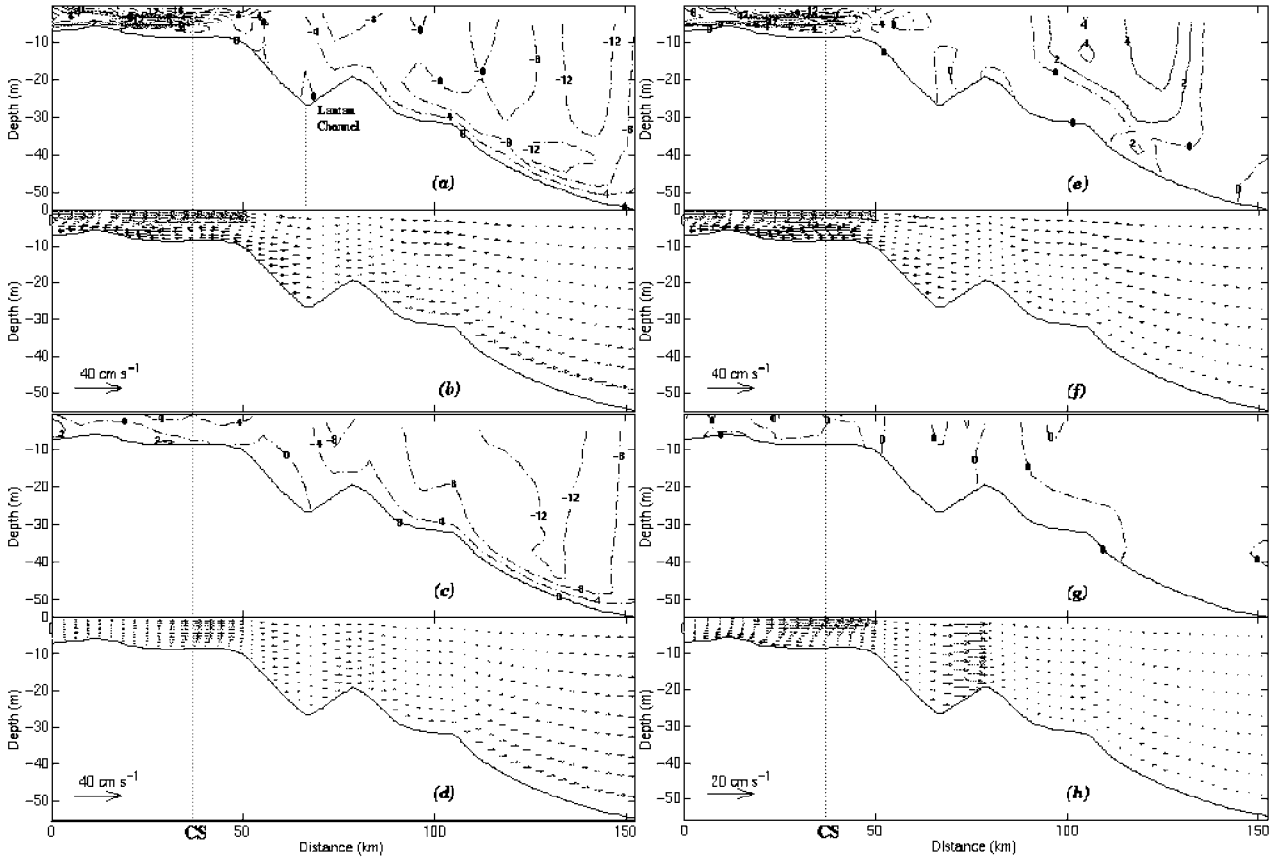

Figure 4. The comparison of the vertical distribution of the winter horizontal circulations along the cross section AL. (a) and (b) The total subtidal circulation, (c) and (d) the ''barotropic'' component of the subtidal circulation, (e) and (f) the ''baroclinic'' component of the subtidal circulation, and (g) and (h) for the subtidal circulation during the spring tide due to nonlinear tidal effects. Figures 4a–4f correspond to the neap tide.

generated through the NSMSCS owing to its climatological open boundary condition.

[18] After adding the tidal forcing, the basic patterns of the residual surface and bottom circulation are similar to those without the tide (Figures 6g and 6h) except in the region near the head of the estuary where the surface down-the-estuary flow weakens and the bottom flow changes from up-the-estuary to down-the-estuary. The reason is that the water column near the head of the estuary becomes well mixed in the presence of tidal mixing. The westward branch is wider although the speed is somewhat reduced. The surface cyclone eddy in the coastal waters west of the PRE still exists even during the spring tide (Figure 6g).

[19] The second group of the summer sensitivity experiments focuses on the effect of the wind. The addition of a moderate southwesterly wind has limited effects on the circulation inside the PRE (Figures 7a and 6g and Figures 7b and 6h). When the wind speed increases to 5 m s^{-1}, the surface outflow turns eastward near the Qiao Island which enhances the surface flow on the eastern site of the PRE, and the bottom intrusion can reach farther north (Figures 7c and 7d). On the other hand, the coastal circulation is greatly changed. The surface westward branch of the diluted water flowing out from the estuary is much reduced with the addition of the southwesterly monsoon, and it disappears entirely when the wind speed exceeds 5 m s^{-1} (Figures 7a and 7c). Most of the diluted water is driven eastward, imposing strong influences on the Hong Kong coastal waters, especially to the west and south of Hong Kong. The plume extends eastward and the salinity can be as low as 28 ppt in the coastal water about 30 kilometers south of Mirs and Daya Bay, although salinity remains high in both bays because they are in the shadow of Kowloon Peninsula (Figure 7c). The weakening of the westward branch in the presence of southwesterly winds is because the northeastward coastal current is greatly enhanced (Figure 7g) and the plume is driven eastward and further entrained in the coastal current such that the flows driven by the density gradient are mostly southeastward in the coastal waters except west of the PRE in a narrow band less than 20 km from the shoreline where the density driven flows are westward (Figure 7e).

[20] In the coastal waters the surface flow has a slight offshore component, which becomes stronger in the plume. The near bottom flow, however, is obviously shoreward (Figure 7d), indicating the coastal upwelling associated with the southwesterly monsoon during the summer. On the other hand, coastal upwelling establishes a cross-shore temperature gradient [see *Wong et al.*, 2003, Figures 10a and 10c], and the corresponding density driven flow is southwestward

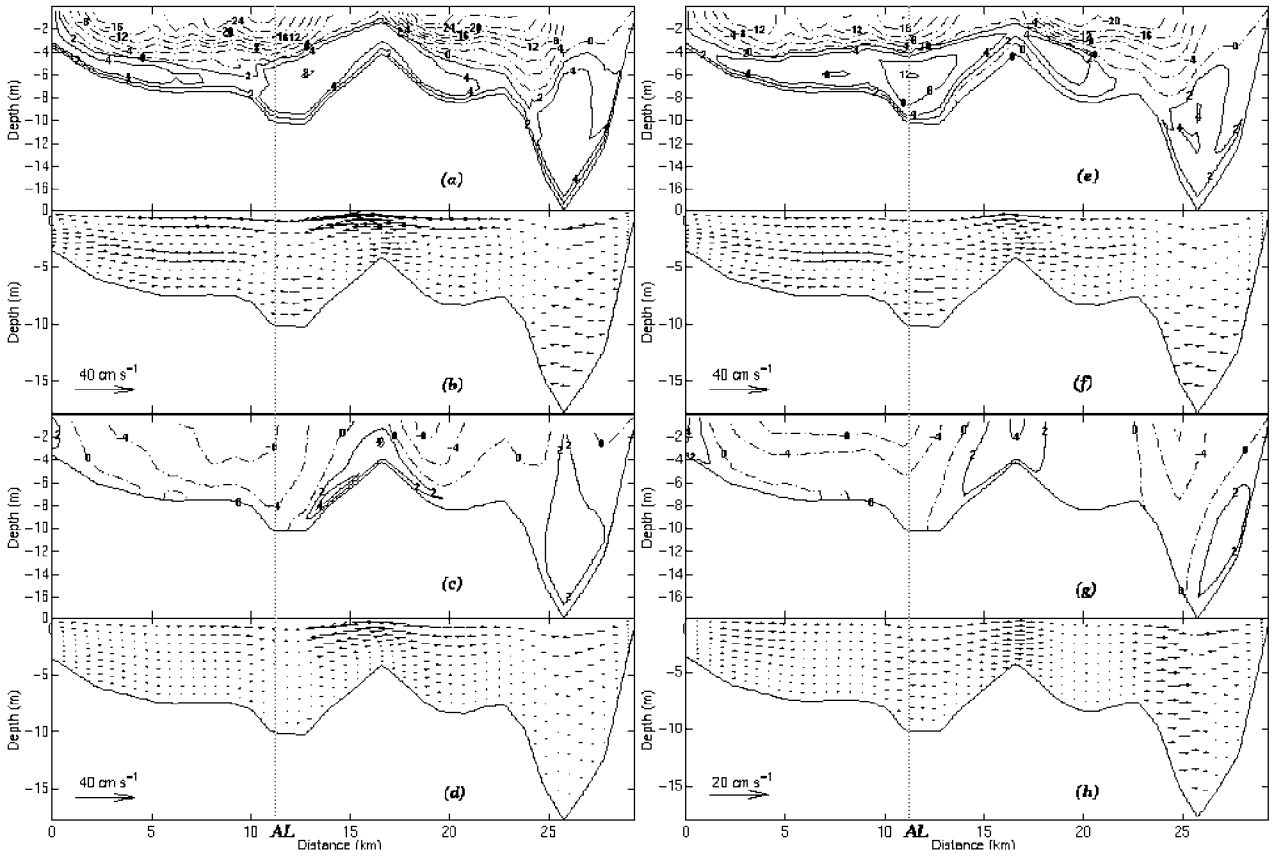

Figure 5. Similar to Figure 4 but for the transversal section CS.

within a distance of ~10 km (i.e., the Rossby radius) from the shoreline as seen in Figure 7e on both sides of the PRE. Near the bottom, the southwestward density driven flow veers offshore when encountering the island chains at the mouth of the PRE (Figure 7f).

4.2. Vertical Features of the Summer Circulation

[21] Figure 8 compares the vertical distribution of the horizontal circulation along the main axial section AL and the transversal section CS (see Figure 3 for the location of AL and CS). Near the head of the estuary, the flow is almost always seaward. The river outflow is, however, concentrated near the surface when tide is absent (Figure 8b). Furthermore, when both the tide and wind are turned off, there is clearly a two-layer gravitational circulation in the estuary with the seaward surface flow and shoreward bottom flow along the main axis of the estuary. Its surface scale is about 90 km from the head to the outside of the estuary and this scale is larger than its counterpart in the winter (see Figure 4b). With the addition of tide, vertical shear of the velocity is much reduced near the head of the estuary because of tidal mixing (Figures 8d and 8f). Northward intrusion of the bottom water is stopped from the inner PRE and the flow is seaward throughout the water column in the inner half (~40 km) of the estuary.

[22] Without the tide and wind, the transversal flow along the main axis of the estuary is small (Figure 8a). The eastward branch of the plume can be found south the Lantau Island with a subsurface maximum of 28 cm s^{-1}. The inclusion of tide results in an eastward surface flow and westward bottom flow inside the estuary (Figures 8c and 8j). Furthermore, the plume front in the coastal water is slightly diffused (not shown), but the effect can be seen from the seaward expansion of the eastward flow as well as the decrease of eastward velocity associated with the plume (Figure 8c). The coastal flow is eastward at about 8 ~ 10 cm s^{-1} in the absence of wind. However, the eastward velocity in the coastal water increases greatly near the surface to more than 30 cm s^{-1} and about 12 cm s^{-1} at depth attributed to the direct wind driven flow and the seaward advection of the plume (Figure 8e).

[23] The transversal cross-section CS (Figures 8g–8l) clearly shows the seaward flow near the surface and the up-the-estuary flow near the bottom when tide and wind are turned off (Figure 8g). Moreover, the surface seaward flow splits into two branches near the Neilingding Island. When tide is added, the bottom intrusion is limited to the eastern side of the two deep channels (Figure 8i). The southwesterly wind, on the other hand, appears to enhance the bottom northward intrusion (Figure 8k). Finally, the inclusion of tide results in stronger eastward surface flow across the estuary, while the inclusion of wind appears to enhance the westward flow at depth.

5. Variability of the Plume Front

[24] In the winter, a sharp salinity gradient exists inside the PRE from northeast to southwest and continuing along

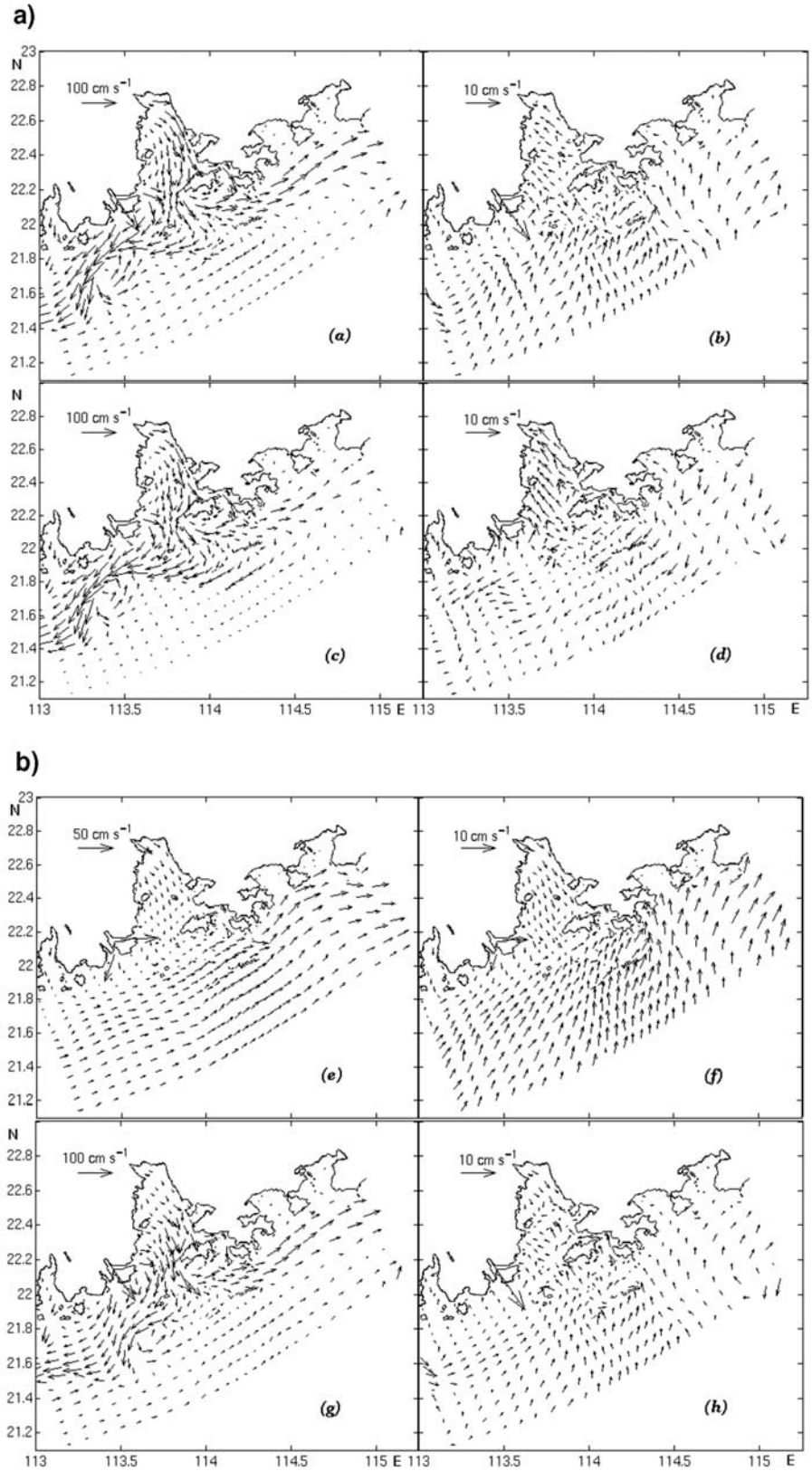

Figure 6. The comparison of the summer surface and bottom circulations without wind. (a) and (b) The special surface and the bottom subtidal circulations without wind and tide, (c) and (d) the surface and bottom baroclinic contribution driven by density gradient without wind and tide, (e) the difference between Figures 6a and 6c, (f) the difference between Figures 6b and 6d, (g) and (h), as in Figures 6a and 6b but with the nonlinear tidal effects during the spring tide. Plot grid interval: 8 grids $\times$ 8 grids.

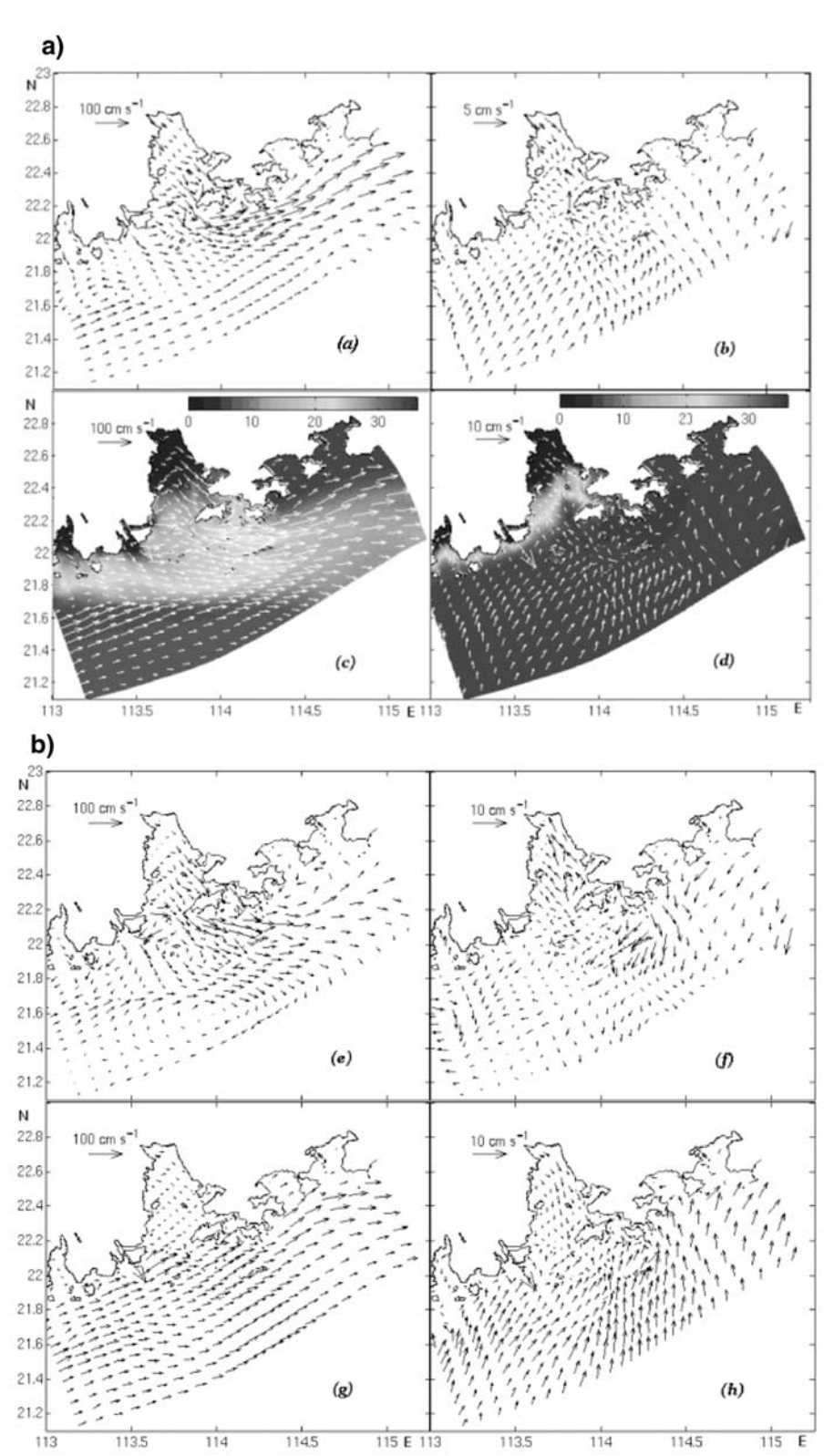

Figure 7. The comparison of the summer surface and bottom circulations during the neap tide with wind. (a) and (b) The summer surface circulation during a westerly monsoon prevailing with wind speed of 3.25 m s^{-1}; (c) and (d) as in Figures 7a and 7b but the wind speed is 5 m s^{-1}; (e) and (f) the baroclinic contribution driven by the density gradient during the southwesterly monsoon prevailing with wind speed of 5 m s^{-1}; and (g) and (h) the rest of the circulation components from that the general circulation (Figures 7c and 7d) minus the density gradient circulation (Figures 7e and 7f). Plot grid interval: 8 grids $\times$ 8 grids. The images show the distribution of the surface salinity.

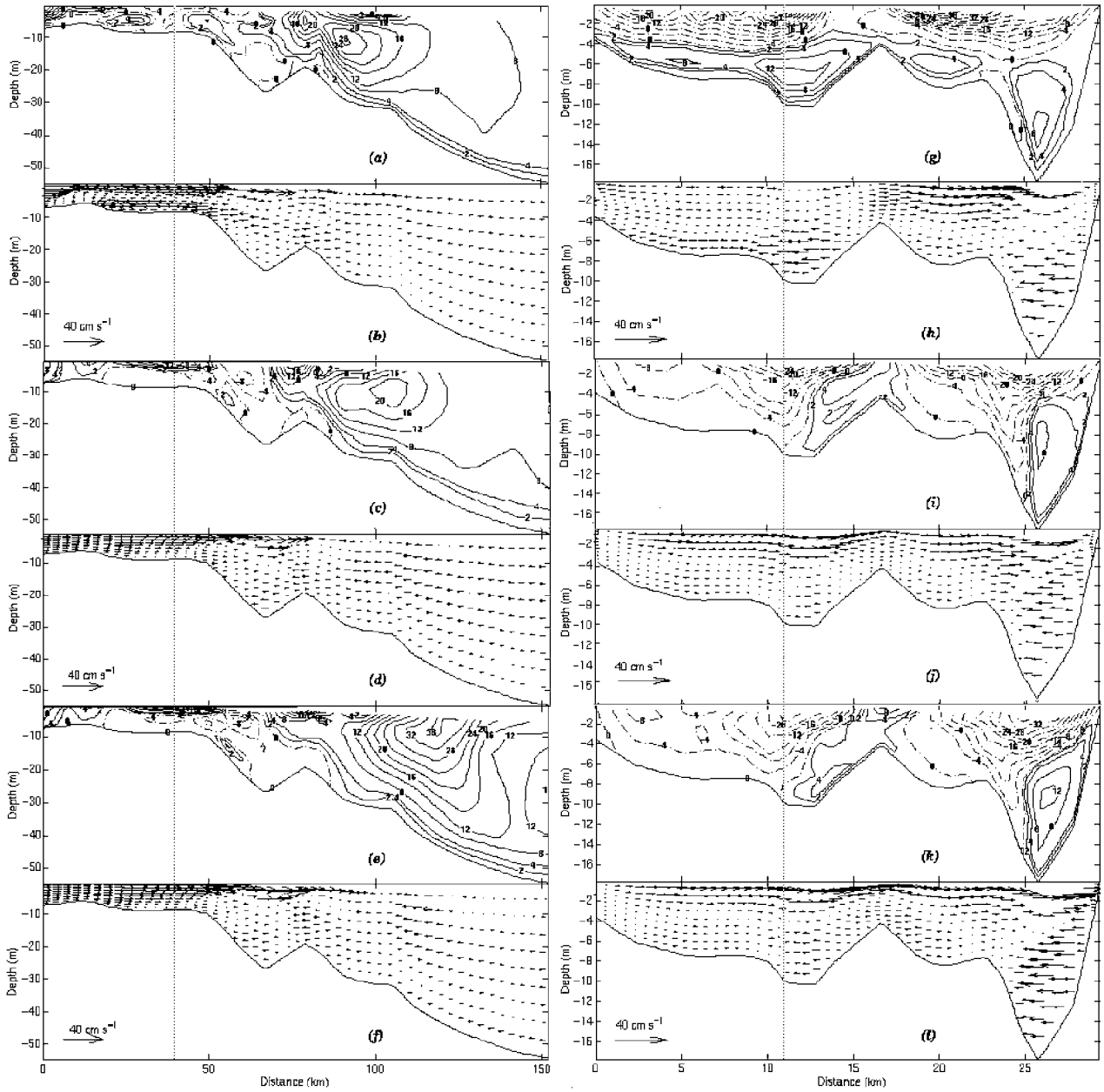

Figure 8. The comparison of the vertical distribution of the summer horizontal circulations along the cross-sections (a)–(f) AL and (g)–(l) CS during the spring tide. Contours show the normal component of the horizontal circulation along the sections and the arrows show the tangential component of the horizontal circulation along the sections; Figures 8a, 8b, 8g, and 8h show the subtidal circulation without wind and tide. Figures 8c, 8d, 8i, and 8j are as in Figures 8a, 8b, 8g, and 8h but with the addition of nonlinear tidal effects; Figures 8e, 8f, 8k, and 8l, are as in Figures 8c, 8d, 8i, and 8j but with the southwesterly monsoon of 5 m s^{-1} is added in the system.

the coast west of the PRE (Figure 2a). In the vertical, the halocline has a small downward-and-northward tilt with a relatively sharper subsurface front even closer to the head of the estuary [see *Wong et al.*, 2003, Figures 9e and 9f]. The seaward discharge of the diluted water and the onshore Ekman transport of the coastal water during the northeasterly wind causes the convergence of the surface water, which sets up a transition zone of strong salinity gradient where the strongest flow is found in the direction perpendicular to the gradient. These characteristics are indicative of the presence of a front that is along the axis of the estuary and the western shoreline outside of the PRE. It is also noted that the intrusion of saline offshore water into the inner estuary occurs in two deep channels, namely, the Urmston Waterway and the West Channel (Figure 2b).

[25] During the summer, wet season, the large river runoff results in the low-salinity water filling the surface layer of the entire estuary and further spreading into the coastal

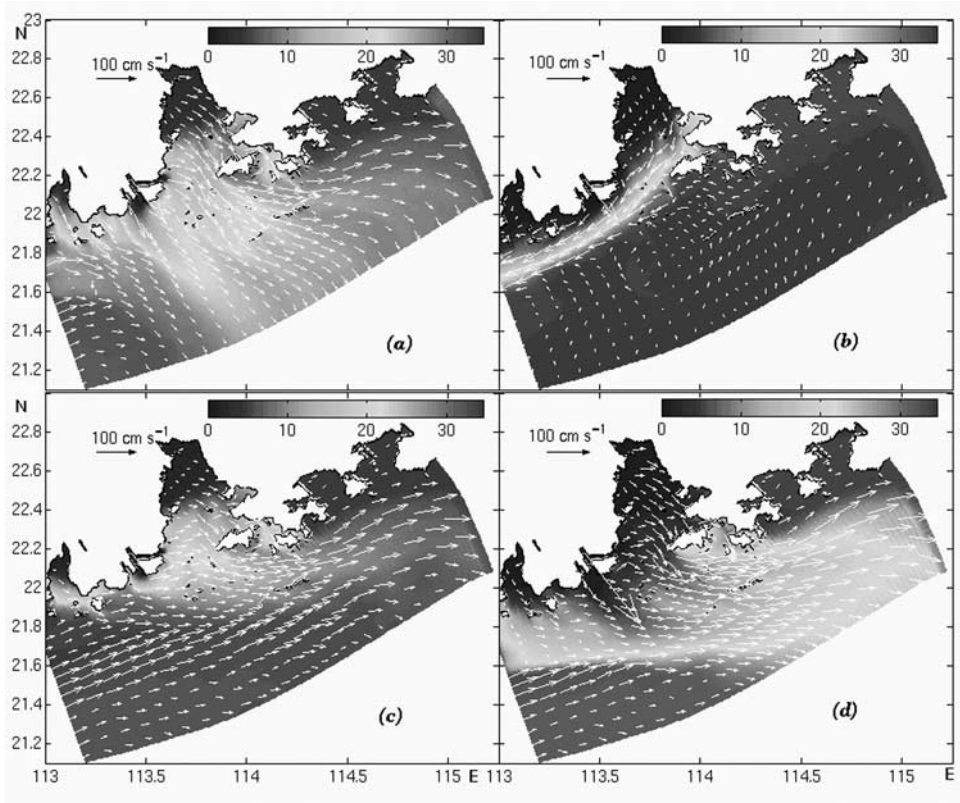

Figure 9. The comparison of the summer surface circulation and river plumes. (a) As shown in Figure 7c but for a westerly wind of 5 m s^{-1}; (b) as shown in Figure 7c but for an easterly wind of 5 m s^{-1}; (c) as in Figure 7c but the river discharge rate is reduced by half; and (d) as in Figure 7c but the river discharge rate is increased to 1.5 times of the monthly average.

waters (Figure 7c). In the coastal water west of the PRE, convergence occurs between the northeastward coastal current and the southeastward plume water to maintain a relatively sharp salinity gradient. In contrast, the plume is entrained in the coastal current east of the PRE where the diluted water forms a salinity tongue extending eastward and frontal characteristics are thus not evident in the surface layer (Figure 7c). However, the frontal characteristics remain near the bottom (Figure 7d). Compared with its winter counterpart, the subsurface salinity front in the PRE and in Huangmaohai Bay moves to near the entrance because of the large discharge in the summer. The halocline is almost horizontal in the vertical plain [see *Wong et al.*, 2003, Figures 9a and 9b] and the vertical gradient of salinity is exceptionally strong. Therefore the misalignment of the surface and bottom fronts is a result of decoupling between the surface and the lower layer in the presence of strong stratification and the surface layer being subject to an offshore Ekman transport. The sensitivity experiments also demonstrate that the spring-neap tidal cycle affects the strength of stratification inside the estuary, but not the basic frontal characteristics.

[26] In general, the coastal circulation pattern varies more in summer than in winter for the summer wind frequently changes its direction and strength in this region [*Yuan et al.*, 1990]. The spreading of the plume in the coastal waters depends largely on the coastal circulation, which in turn depending on the direction and magnitude of the prevailing wind. In addition, the river discharge also plays an important role in controlling the plume and the frontal structure. A westerly wind appears to increase the seaward spreading of the plume (Figure 9a), while the easterly wind produces a westward plume, very much like the winter scenario except that the front is now in the coastal water instead of hugging the western shoreline (Figure 9b) because of the overly large discharge. The eastward spreading of the plume is clearly a result of the southwesterly wind component since it occurs in all three experiments with the southwesterly wind although the discharge varies from 0.5 (Figure 9c), 1.0 (Figure 7c), and 1.5 (Figure 9d) times the normal rate. Furthermore, the plume is always entrained in the coastal current, which produces a low-salinity tongue extending eastward. The difference between the three experiments is the size of the plume directly proportional to the amount of discharge, for example, plume area (covered by the surface salinity $\leq$26 ppt) associated with the three experiments (Figures 9c, 7c, and 9d) is about 3,250 km^2, 7,330 km^2, and 13,300 km^2, respectively.

6. Conclusions

[27] The dynamics of the winter and summer circulations in the PRE and its coastal waters is examined by using the 3D POM. Results from the sensitivity experiments show the following.

[28] 1. The seaward spreading of the plume water and the onshore Ekman transport of the marine water induced by the northeasterly wind in the winter sets up a sharp salinity front

that aligns from the northeast to the southwest in the PRE. The front separates the low-salinity plume water in the northwest of the estuary from the saline marine water in the southeast. The asymmetry is due to the discharges being all on the west bank of the PRE and the subsequent steering effect by the Coriolis force.

[29] 2. The frontal dynamics associated with the river plume controls the circulation inside the PRE. The surface currents tend to concentrate along the salinity front in the axial direction of the estuary and flow toward the sea, while the bottom currents flow toward the head of the estuary along two deep channels. This two-layer gravitational circulation is mostly driven by the density gradient. The intrusion at depth pushes the subsurface front toward the head of the estuary such that the halocline tilts upward and seaward, although the tilt is smaller in the winter as compared to that in the summer.

[30] 3. During the summer, the plume water fills the PRE at the surface and spills into the coastal waters. During the prevailing southwesterly monsoon in the summer, the seaward spreading of the plume water converges with the northeastward coastal current and forms a moderate salinity front to the southwest of the mouth of the PRE. In contrast, to the east of the PRE the plume is entrained in the coastal current and extends eastward as a low-salinity tongue with much weaker salinity gradient. The overall alignment of the plume is from northwest to southeast.

[31] 4. The bottom front moves from near the head of the PRE during the winter low discharge season to near the mouth of the PRE during the summer high discharge season. However, the overall alignment is from northeast to southwest, similar to that in the winter. The misalignment between the surface and the bottom front can be attributed to the decoupling between the surface and subsurface waters by the strong vertical stratification, result from the overly large discharge and the seaward advection of the surface plume driven by the wind.

[32] 5. The coastal circulation, thereby the spread of the river plume in the coastal waters, highly depends on the wind direction. A westerly wind enhances seaward spreading of the plume, whereas an easterly wind drives the plume toward the west, similar to the winter situation. The eastward spreading of the plume can be attributed to the southwesterly monsoon. The area of the plume, however, is positively proportional to the amount of discharge.

[33] **Acknowledgments.** The present study was supported by the Pearl River Estuary Pollution Project funded by the Hong Kong Special Administrative Region Government/Hong Kong Jockey Club, and by the 863/818-09-01 grant from the Ministry of Science and Technology of China.

References

Chen, Z. Y., *Tide Dynamics*, pp. 196–197, China Sci. Press, Beijing, 1980.

Hu, S., Numerical modeling of the Pearl River Estuary, Ph.D. thesis, Dept. of Mech. Eng., Hong Kong Univ. of Sci. and Technol., Hong Kong, China, 1995.

Huang, B. X., Z. S. Guao, K. K. Xian, B. Yu, and F. Huang, Numerical simulation of tidal current of the Pearl River Estuary, *Chin. J. Oceaonol. Limnol.*, *23*, 475–484, 1992.

Wang, J., G. Yu, and Z. Chen, Numerical simulation of tidal current in Neilingding Yang of the Pearl River Estuary, *Acta Oceanol.*, *14*, 26–34, 1992.

Wong, L. A., J. C. Chen, H. Xue, L. X. Dong, J. L. Su, and G. Heinke, A model study of the circulation in the Pearl River Estuary (PRE) and its adjacent coastal waters: 1. Simulations and comparison with observations, *J. Geophys. Res.*, *108*, doi:10.1029/2002JC001451, in press, 2003.

Ye, J., Z. He, and Z. Zhou, Numerical model of salt transport under tidal current for the Pearl River Estuary, *Renmin Zhujiang*, *6*, 7–15, 1986.

Ye, L., and K. D. Preiffer, Studies of 2D & 3D numerical simulation of Kelvin tide wave in Neilingding Yang at the Pearl River Estuary, *Ocean Eng.*, *8*, 33–44, 1990.

Yuan, Z., D. Huang, L. Guan, X. Deng, Meteogological analysis, 1975–1984 Hydrologic Investigation Report for the North Shelf of South China Sea, edited by Y. L. Ma, pp. 16–22, China Ocean Press, Beijing, 1990.

J. C. Chen, W. B. Guan, and L. A. Wong, Center for Coastal and Atmospheric Research, Hong Kong University of Science and Technology, Clear Water Bay, Kowloon, Hong Kong. (wla@ust.hk)

L. X. Dong and J. L. Su, Marine Modeling Laboratory, Second Institute of Oceanography, State Oceanic Administration, P. O. Box 1207, Hangzhou, 310012 China. (donglx@mail.hz.zj.cn)

H. Xue, School School of Marine Sciences, University of Maine, 5741 Libby Hall, Orono, ME 04469-5741, USA. (hxue@maine.edu)